Microstructure, AC impedance and DC electrical conductivity characteristics of $NiFe_{2-x}Gd_xO_4$ (x = 0, 0.05 and 0.075)

Cite as: AIP Advances **2**, 012139 (2012); https://doi.org/10.1063/1.3687219
Submitted: 16 November 2011 . Accepted: 25 January 2012 . Published Online: 08 February 2012

K. Kamala Bharathi, G. Markandeyulu, and C. V. Ramana

Microstructure, AC impedance and DC electrical conductivity characteristics of $NiFe_{2-x}Gd_xO_4$ (x = 0, 0.05 and 0.075)

K. Kamala Bharathi,[1,a] G. Markandeyulu,[2] and C. V. Ramana[3]
[1]*Functional Oxide Thin Film Laboratory, Department of Physics, KAIST, Daejeon - 305701, South Korea*
[2]*Advanced Magnetic Materials Laboratory (AMMLa) Department of Physics, Indian Institute of Technology Madras, Chennai - 600 036, India*
[3]*Department of Mechanical Engineering, University of Texas at El Paso, El Paso, Texas 79968, USA*

(Received 16 November 2011; accepted 25 January 2012; published online 8 February 2012)

The structure and electrical characteristics of Gd doped Ni ferrite materials, namely $NiFe_{1.95}Gd_{0.05}O_4$ and $NiFe_{1.925}Gd_{0.075}O_4$, are reported to demonstrate their improved electrical properties compared to that of pure $NiFe_2O_4$. $NiFe_{1.95}Gd_{0.05}O_4$ and $NiFe_{1.925}Gd_{0.075}O_4$ compounds crystallize in the cubic inverse spinel phase with a very small amount of $GdFeO_3$ additional phase while pure $NiFe_2O_4$ crystallize in inverse spinel phase without any impurity phase. The back scattered electron imaging analysis indicate the primary and secondary formation in $NiFe_{1.95}Gd_{0.05}O_4$ and $NiFe_{1.925}Gd_{0.075}O_4$ compounds. Atomic force microscopy measurements indicate that the bulk grains are ~2-5 micron size while the grain boundaries are thin compared to bulk grains. Impedance spectroscopic analysis at different temperature indicates the different relaxation mechanisms and their variation with temperature, bulk grain and grain-boundary contributions to the electrical conductivity (R_g) and capacitance (C_g) of these materials. The conductivity in pure $NiFeO_4$ is found to be predominantly due to intrinsic bulk contribution (R_g=213 kΩ and C_g=4.5 x 10^{-8} F). In the case of $NiFe_{1.95}Gd_{0.05}O_4$ and $NiFe_{1.925}Gd_{0.075}O_4$ compounds, grain and grain-boundary contributions to the conductivity are clearly observed. The DC conductivity values (at 300 K) of $NiFe_2O_4$, $NiFe_{1.95}Gd_{0.05}O_4$ and $NiFe_{1.925}Gd_{0.075}O_4$ compounds are found to be 1.06 x 10^{-7} Ω^{-1} cm^{-1}, 5.73 x 10^{-8} Ω^{-1} cm^{-1} and 1.28 x 10^{-8} Ω^{-1} cm^{-1} respectively. [doi:10.1063/1.3687219]

I. INTRODUCTION

Ferrite materials, which are magnetic and insulating oxides, have been received significant attention in recent years due to their wide range of applications[1–29] in the current and emerging technological applications in solid oxide fuel cells, ultrahigh-density magnetic, magneto-optical recordings, etc.[1–29]

Nickel (Ni) ferrite crystallizes in inverse spinel phase.[1,2] The tetrahedral (A) sites are occupied by the Fe^{3+} ions and the octahedral sites (B) are occupied by the Ni^{2+} and Fe^{3+}, in equal proportions. Ni ferrite has high saturation magnetization, high Curie temperature, large permeability at high frequency, and remarkably high electrical resistivity.[1–29] Due to their low eddy current losses, no other materials exist with such a high merit to the electronic applications in terms of power generation, conditioning, and conversion.[1–29] These properties also make them unique for application in microwave devices which require strong coupling to electromagnetic signals.

[a]Author to whom correspondence should be addressed; E-mail: kbkaruppanan@utep.edu

Recently, a considerable attention has been paid towards the magnetic and electrical properties of metal doped spinel ferrites (Ni, Co, Ni-Zn, Zn ferrite).[12–31] However, the efforts towards understanding the effect of the substitution of rare earth (R) ions in spinel oxides are meager. Engineering the materials and development of devices for high frequency applications based on nickel ferrites is clearly dependent upon the fundamental knowledge of electrical behavior of these materials. Therefore, the present work has been focused on structural, AC impedance and electrical properties of Gd doped Ni ferrites along with a comparison of the data of pure Ni ferrite.

Impedance spectroscopy (IS), which is the primary tool in this work, is the analytical tool to study the dielectric properties of ferrites, since impedance of the grains can be divided from other impedance sources, such as impedance of electrodes, impurity phases and grain boundaries.[32–34] Several factors such as microstructure, doping element and doping concentration can influence the electrical impedance properties of ferrites.[32–34] Usually, the changes in microstructure as a result of doping also changes the resistivities of ferrites.[35,36] The electrical resistivities are important as high resistivity can reduce eddy current losses which become increasingly important as the operating frequency of nickel ferrites is raised. Depending upon the ion size and amount, the dopants may either substitute within the spinel ferrite, or so alter the bulk resistivity, or they may segregate to grain boundaries, and so alter the grain boundary resistivities. Impedance spectroscopic analysis allows the determination of contributions of dopants/additives to the grain boundary resistivity and bulk resistivity to be separated with an end result that such an analysis can be used to provide more information on the role of the doping elements on the electrical properties. The results obtained on the pure and Gd substituted Ni ferrites are presented. In addition, variation of electrical properties with increasing Gd substitution is also discussed in this paper.

II. EXPERIMENTAL SECTION

The materials were prepared using the conventional solid state chemical reaction method. The starting materials were 99.99% pure NiO, Fe_2O_3 and Gd_2O_3. Powders of the starting materials were ground in a mortar and pestle for one hour and the mixtures were heat treated in air at 1200 °C for 12 hours. The powders made into pellets and then sintered at 1250 °C in air for 12 hours were employed for electrical measurements. The XRD patterns of the samples were obtained at room temperature using a PANalytical (X'pert PRO) x-ray diffractometer employing Cu Kα radiation (1.54 Å). Surface morphology and backscattered electron (BSE) image analysis was performed using a high-performance and ultra high resolution scanning electron microscope (Hitachi S-4800). Surface characterization and grain size analysis was performed using Atomic Force Microscopy (AFM) employing Nanoscope IV-Dimension 3100 SPM system. Dielectric and impedance measurements were carried out employing impedance analyzer (HP 4192A).

III. RESULTS AND DISCUSSION

Figure 1(a) shows the XRD patterns of the pure Ni ferrites. The data indicate that the materials crystallize in the inverse spinel phase without any impurity phase. The calculated lattice constant for pure Ni ferrite is 8.335 Å, which agrees with the reported value.[1,2,37] Fig. 1(b) and 1(c) shows the XRD patterns of $NiFe_{1.95}Gd_{0.05}O_4$ and $NiFe_{1.925}Gd_{0.075}O_4$ compounds, respectively. XRD data reveal that $NiFe_{1.95}Gd_{0.05}O_4$ and $NiFe_{1.925}Gd_{0.075}O_4$ materials also crystallize in the inverse spinel phase. Very small amounts of $GdFeO_3$ phases were identified in both the compounds. The calculated lattice constant values for $NiFe_{1.95}Gd_{0.05}O_4$ and $NiFe_{1.925}Gd_{0.075}O_4$ compounds are 8.346 Å and 8.343 Å, respectively. The lattice constant of Gd doped compounds are found to be larger than that of pure Ni ferrite due to the larger ionic size of Gd^{3+}. The weight fractions of the inverse spinel phase and $GdFeO_3$ are 0.938 and 0.062, 0.924 and 0.076 for $NiFe_{1.95}Gd_{0.05}O_4$ and $NiFe_{1.925}Gd_{0.075}O_4$, respectively. Small distortion in the lattice is observed upon the substitution of Fe by Gd in the B site from the changes in Fe-O–Fe, R–O–Fe, R–O-Ni bond angles and bond lengths (O–Fe and O–Ni bond lengths) in the B site compared to $NiFe_2O_4$.[1] The detailed analysis of the XRD data and refined structural details are shown in Table I.

TABLE I. Refined values of Bond angle, bond length of $NiFe_2O_4$, $NiFe_{1.95}Gd_{0.05}O_4$ and $NiFe_{1.925}Gd_{0.075}O_4$.

Compound	Fe^{3+} – O – Fe^{3+} (Gd^{3+}) Bond angle (degrees)	Ni^{2+} – O – Ni^{2+} Bond angle (degrees)	O – Fe^{3+} (Gd^{3+}) Bond length (Å)
$NiFe_2O_4$	159.2	90.6	2.050
$NiFe_{1.95}Gd_{0.05}O_4$	157.3	90.2	2.179
$NiFe_{1.925}Gd_{0.075}O_4$	157.6	90.3	2.181

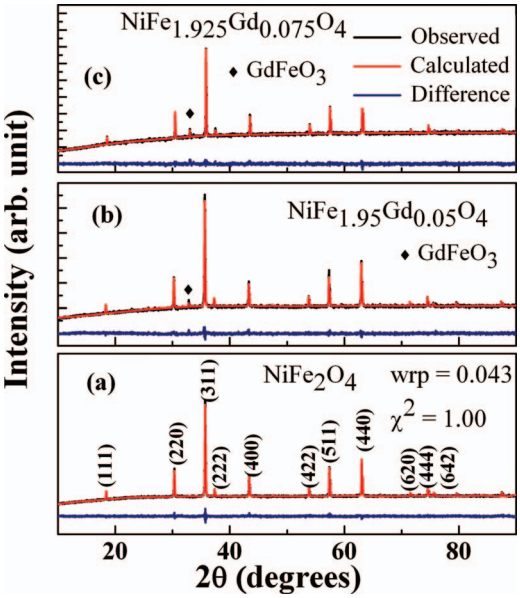

FIG. 1. XRD patterns of $NiFe_2O_4$ (a), $NiFe_{1.95}Gd_{0.05}O_4$ (b), $NiFe_{1.925}Gd_{0.075}O_4$ (c). The calculated pattern obtained after the Rietveld refinement and the differences are also shown.

The BSE images of $NiFe_{1.95}Gd_{0.05}O_4$ and $NiFe_{1.925}Gd_{0.075}O_4$ compounds are shown in Fig. 2. These images indicate two distinct contrasts correspond to their respective primary parent (spinel) phase and the secondary $GdFeO_3$ phases of $NiFe_{1.95}Gd_{0.05}O_4$ and $NiFe_{1.925}Gd_{0.075}O_4$ compounds. The particles corresponding to the small amount of secondary phase are as shown in Fig. 2 with arrows. Substitution of small amount of Gd for Fe at B site of their parent phases has been confirmed from the EDX measurements (not shown).

The AFM images of $NiFe_{1.95}Gd_{0.05}O_4$ and $NiFe_{1.925}Gd_{0.075}O_4$ compounds are shown in Fig. 3. It is evident that the larger grains are separated by thin grain boundaries and the grains are 1-2 μm in size (Fig. 3). The images also reveal that the grain boundaries are very thin compared to the bulk of the grains.

The impedance of $NiFe_2O_4$, $NiFe_{1.95}Gd_{0.05}O_4$ and $NiFe_{1.925}Gd_{0.075}O_4$ was measured in the frequency range 10 Hz - 13 MHz (at 300 – 343 K). Impedance of a polycrystalline ferrite material can be expressed as[2,27,38]

$$Z = Z' + jZ'' = R + \frac{1}{j\omega C} \tag{1}$$

Where

$$Z' = \frac{1/R}{(1/R^2) + \omega^2 C^2} \tag{2}$$

$$Z'' = \frac{-\omega C}{1/R^2 + \omega^2 C^2} \tag{3}$$

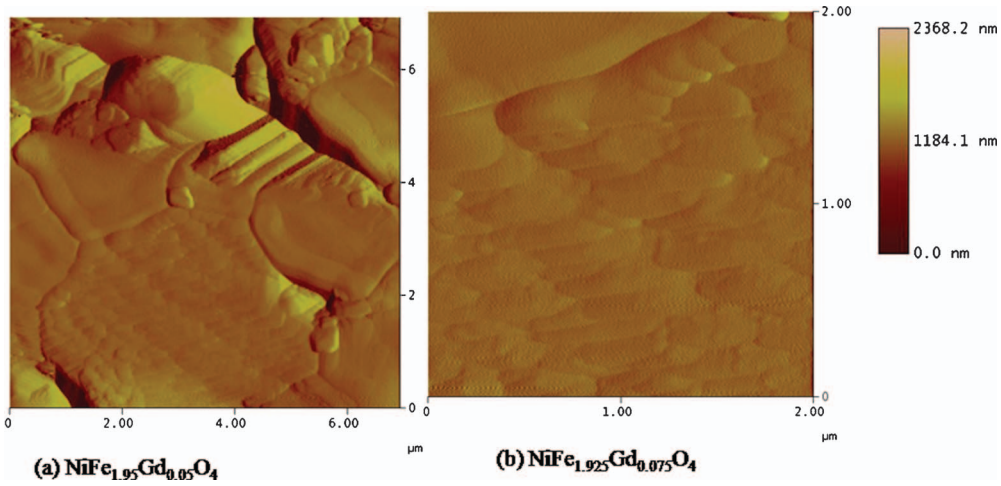

FIG. 2. AFM images of $NiFe_{1.95}Gd_{0.05}O_4$ (a), $NiFe_{1.925}Gd_{0.075}O_4$ (b). AFM images indicates that the grains are very large (micron size) compare to the thin grain boundaries.

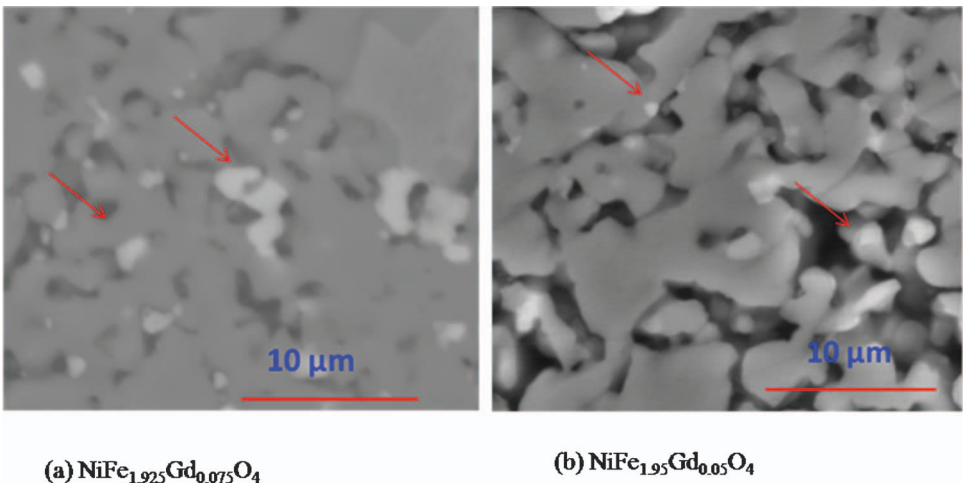

FIG. 3. BSE images of $NiFe_{1.925}Gd_{0.075}O_4$ (a), $NiFe_{1.95}Gd_{0.05}O_4$ (b). Secondary phase is indicated in red arrow.

Variation of real part of impedance (Z') with frequency at selected temperatures for $NiFe_2O_4$, $NiFe_{1.95}Gd_{0.05}O_4$ and $NiFe_{1.925}Gd_{0.075}O_4$ is shown in Fig. 4. Z' is seen to decrease with increasing frequency. This observation indicates that the conductivity of these materials increases as the frequency increases. Such behavior can be attributed to the increased hopping of electrons between the localized ions.

Figure 5 shows the imaginary part of impedance (Z'') as a function of frequency at different temperatures. Z'' decreases with increasing frequency and temperature. In addition, the broad Debye peaks noticed Z'' indicative of the relaxation processes in these materials. Debye peaks appear when the hopping frequency of localized electrons becomes equal to the frequency of the applied electric field. Observation of relaxation peaks at low frequencies in the Z'' part of complex impedance is due to the existence of the space–charge relaxation, associated with the charge carriers resulting from oxygen vacancies. Space charge polarization is known to dominate when the material is composed of grain and grain boundaries.[2,39–41] With increasing temperature, Debye peaks are seen to move to the higher frequency side due to an increase in the rate of hopping of electrons. Also, Z'' decreases with increasing temperature due to the decreasing loss in the resistive part of the sample.

Figure 6 shows the Cole-Cole plot (real (Z') *versus* imaginary (Z'') part of impedance) of pure Ni ferrite at room temperature. The Cole-Cole plot exhibits a semi-circle, which is typically assumed

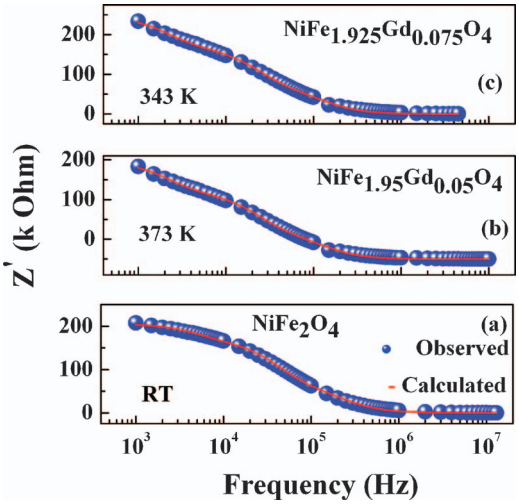

FIG. 4. Frequency variation of real part of impedance (Z') of $NiFe_2O_4$, $NiFe_{1.95}Gd_{0.05}O_4$ and $NiFe_{1.925}Gd_{0.075}O_4$.

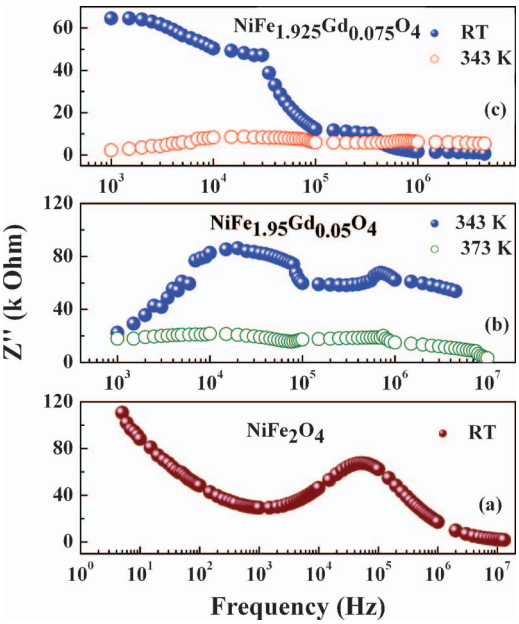

FIG. 5. Frequency variation of imaginary part of impedance (Z'') (at different temperatures) of $NiFe_2O_4$, $NiFe_{1.95}Gd_{0.05}O_4$ and $NiFe_{1.925}Gd_{0.075}O_4$.

to account for the intrinsic bulk grain contribution to the resistance (R_g) and capacitance (C_g). Impedance can be expressed as:[2,27,30]

$$Z = R_g + \frac{1}{i\omega C_g} \tag{4}$$

The value of R_g was obtained from the diameter of the semi circle and C_g was calculated using the relation ωRC=1, at maximum Z″ point in semicircle. The calculated value of R_g is 213 kΩ and that of C_g is 4.5 x 10^{-8} F. The contribution from the grain boundary could not be resolved in the case of pure Ni ferrite. The relaxation time τ_g=0.00958 s is calculated from the relation:

$$\tau_g = \frac{1}{\omega_g} = R_g C_g \tag{5}$$

TABLE II. Resistance, capacitance and relaxation time values corresponds to grain and grain boundaries of $NiFe_2O_4$, $NiFe_{1.95}Gd_{0.05}O_4$ and $NiFe_{1.925}Gd_{0.075}O_4$.

Compound	R_g kΩ	C_g (10^{-8} F)	τ_g (μs)	R_{gb} kΩ	C_{gb} (10^{-8} F)	τ_{gb} (μs)
T = 343 K $NiFe_{1.925}Gd_{0.075}O_4$	253	3.2	118	192	3.1	61
T = 343 K $NiFe_{1.95}Gd_{0.05}O_4$	248	3.3	107	188	3.3	59
T=373 K $NiFe_{1.95}Gd_{0.05}O_4$	72	2.9	98	57	2.7	46

In the case of $NiFe_{1.95}Gd_{0.05}O_4$ and $NiFe_{1.925}Gd_{0.075}O_4$ compounds, room temperature Cole-Cole plots exhibit incomplete semicircles due to the high resistance values at low frequencies. Two semicircles can be observed for both the compounds (Fig. 7 and 8) with increasing temperature above 330 K. The origin of the second semicircle is attributed to the formation of small amounts of $GdFeO_3$ phase, which segregate at grain boundaries and contribute additionally to the grain boundary scattering. Each semi-circle corresponds to resister-capacitor RC phase. Such an analysis is certainly very helpful to represent the sample by an electrical circuit as a combination of resistors and capacitors as shown in Fig. 9. In this circuit, capacitances will be associated with space charge region and a resistance represents a conductive path and a given resistor in a circuit might account for the bulk conductivity of the sample. Analytically impedance can be expressed as:

$$Z = R_g + \frac{1}{j\omega C_g} + R_{gb} + \frac{1}{j\omega C_{gb}} \tag{6}$$

$$Z' = \frac{R_g}{\left(1 + \omega_g C_g R_g\right)^2} \frac{R_{gb}}{\left(1 + \omega_{gb} C_{gb} R_{gb}\right)^2} \tag{7}$$

$$Z'' = \frac{-R_g^2 \omega_g C_g}{1 + \left(\omega_g C_g R_g\right)^2} + \frac{-R_{gb}^2 \omega_{gb} C_{gb}}{1 + \left(\omega_{gb} C_{gb} R_{gb}\right)^2} \tag{8}$$

where R_{gb} and C_{gb} represents the resistance and capacitance of the grain boundary volume. AFM measurements (Fig. 3) revealed the fact that the grains are very large compare to the thin grain boundaries. Therefore, the contribution from the grains to the resistance and the capacitance must be large compare to that of the smaller and thin grain boundaries. Therefore, the larger semi circle in the Cole-Cole plot at low frequency side is attributed to the larger grains and the small semi circle at high frequency side attributed to the grain boundaries. The calculated values of R_g, C_g, R_{gb}, C_{gb}, τ_g and τ_{gb} at various temperatures for all the compounds are shown in Table II. Relaxation time of grain boundaries τ_{gb} is found to be smaller compared to that of grains. This is due to the smaller R_{gb} and C_{gb} values compared to that of R_g and C_g.

Conductivity value of $NiFe_2O_4$, $NiFe_{1.95}Gd_{0.05}O_4$ and $NiFe_{1.925}Gd_{0.075}O_4$ compounds at 300 K was found to be 1.06 x 10^{-7} Ω^{-1} cm^{-1}, 5.73 x 10^{-8} Ω^{-1} cm^{-1} and 1.28 x 10^{-8} Ω^{-1} cm^{-1}, respectively. DC conductivity (resistivity) of $NiFe_2O_4$ decreases (increases) with increasing Gd doping. Substitution of small amounts of Gd^{3+} ions for Fe^{3+} ions in B site increases the inter-ionic distances and distorts the lattice due to larger ionic size of Gd^{3+} compared to that of Fe^{3+} leading to additional scattering and causing increase of resistivity. In addition, formation of small amount of secondary phase ($GdFeO_3$) at the grain boundaries contributes to the increase in the electrical resistivity.

The temperature variation of DC electrical conductivity of $NiFe_2O_4$, $NiFe_{1.95}Gd_{0.05}O_4$ and $NiFe_{1.925}Gd_{0.075}O_4$ is shown in Fig. 10. Electrical conductivity decreases exponentially with decreasing the temperature from 300 K to 120 K which indicates the insulating nature of the compounds. Conductivity in insulators is due to both hopping of electrons and charge transport via excited states

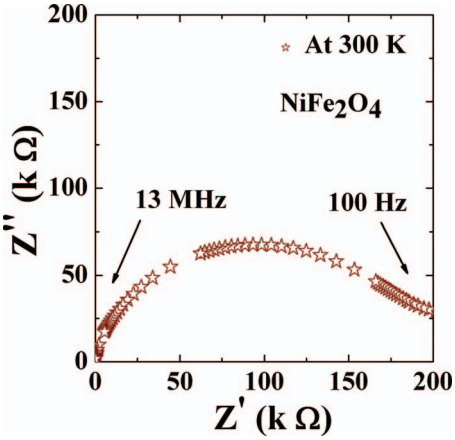

FIG. 6. Cole-Cole plot of $NiFe_2O_4$ at 300 K.

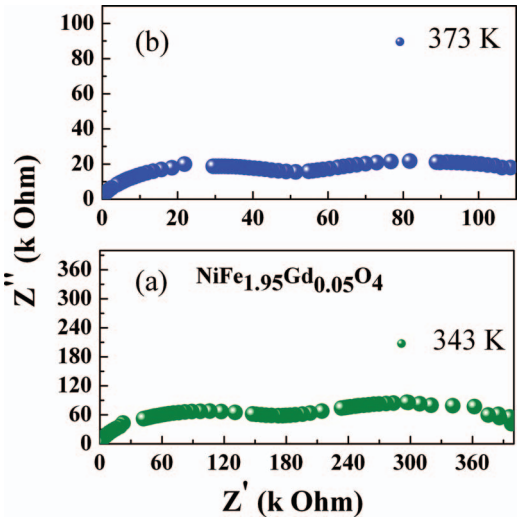

FIG. 7. Cole-Cole plot of $NiFe_{1.925}Gd_{0.05}O_4$ at different temperatures. Decrease in the radius of the semi-circle with increasing temperature is evident.

and it can be expressed as:[42,43]

$$\sigma = A_1 \exp\left(\frac{-E_1}{k_B T}\right) + A_2 \exp\left(\frac{-E_2}{k_B T}\right) + A_3 \exp\left(\frac{-E_3}{k_B T}\right) + \ldots \quad (9)$$

where E_1 is the activation energy for intrinsic conduction and E_2, E_3, ... are the activation energies needed for hopping conduction. A_1, A_2, A_3 are constants and k_B is the Boltzmann constant.

It is evident from the DC electrical conductivity plot (Fig. 10) that two different slopes exists for all the compounds indicating that the conduction is through an activated process having two difference conduction mechanisms. Activation energy values (300-250 K and 250-150 K) were calculated from the lnσ *vs* 1000/T plot and are listed in Table III. Activation energy values were found to be higher at 300-250 K region (0.29 eV for $NiFe_2O_4$) and smaller at 250-150 K region (0.06 eV). Decreasing activation energy with decreasing temperature has been accounted by small-polaron theory.[42,43] The VRH[42,43] model of small polarons also predicts continuously decreasing activation energy with decreasing temperature.

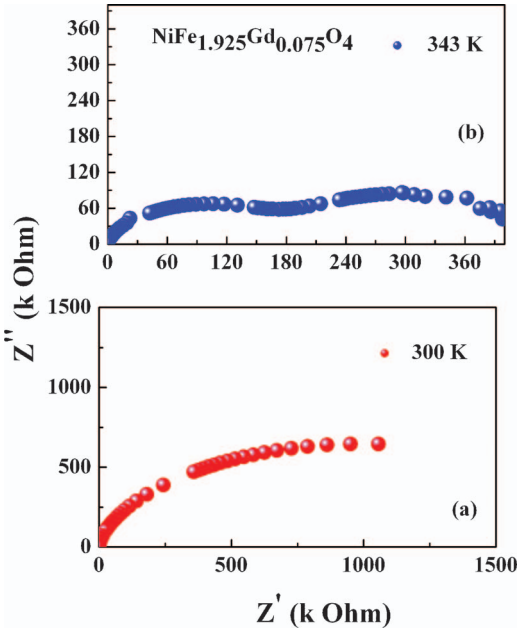

FIG. 8. Cole-Cole plot of $NiFe_{1.925}Gd_{0.075}O_4$ at different temperatures.

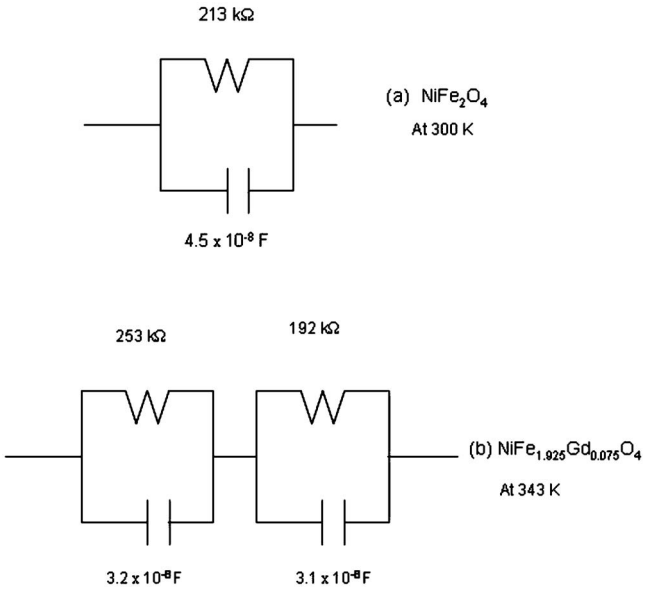

FIG. 9. Equivalent circuits of $NiFe_2O_4$ (a) and $NiFe_{1.925}Gd_{0.075}O_3$ (b).

TABLE III. Activation energy values of $NiFe_2O_4$, $NiFe_{1.95}Gd_{0.05}O_4$ and $NiFe_{1.925}Gd_{0.075}O_4$ at different temperature regions.

Compound	Activation Energy (eV)	
	300 – 250 K	250 – 150 K
$NiFe_2O_4$	0.29	0.06
$NiFe_{1.95}Gd_{0.05}O_4$	0.36	0.08
$NiFe_{1.925}Gd_{0.075}O_4$	0.38	0.09

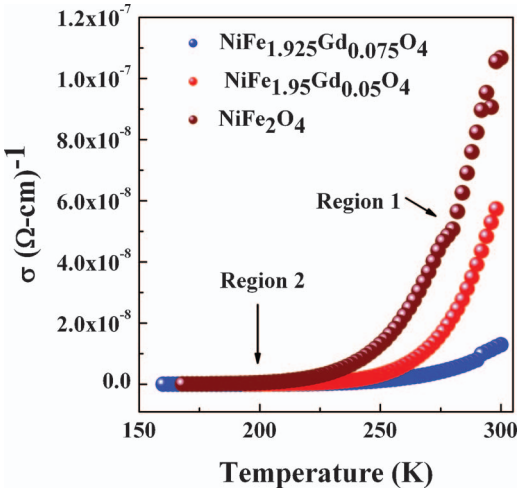

FIG. 10. Temperature variation of conductivity of $NiFe_2O_4$, $NiFe_{1.95}Gd_{0.05}O_4$ and $NiFe_{1.925}Gd_{0.075}O_4$. Two different slope regions are evident in all the curves.

IV. CONCLUSIONS

Substitution of small amount of of Gd^{3+} for Fe^{3+} improves the DC electrical resistivity and impedance properties of Ni ferrite. $NiFe_{1.95}Gd_{0.05}O_4$ and $NiFe_{1.925}Gd_{0.075}O_4$ compounds crystallize in the cubic inverse spinel phase with a very small amount of $GdFeO_3$ additional phase. Real (Z') and imaginary part (Z'') of the impedance decreases with increasing frequency. Z'' exhibits broad Debye peaks indicative of relaxation processes in these materials. Structural studies (AFM and BSE imaging) confirm that $NiFe_{1.95}Gd_xO_4$ (x=0.05 and 0.075) exhibit two different phases. The bulk grains are ~2-5 micron size while the grain boundaries are thin compared to bulk grains. Impedance spectroscopic analysis at different temperature indicates: (a) the different relaxation mechanisms and their variation with temperature and (b) bulk of grain and grain-boundary contributions to the electrical conductivity (R_g) and capacitance (C_g) of these materials. The conductivity in pure $NiFeO_4$ is found to be predominantly due to intrinsic bulk contribution (R_g=213 kΩ and C_g=4.5 x 10^{-8} F). However, in the case of $NiFe_{1.95}Gd_xO_4$ (x=0.05 and 0.75) compounds, grain and grain-boundary contributions are clearly observed. The DC electrical conductivity data confirms the resistivity increase of Ni ferrite upon Gd^{3+} substitution.

[1] S. Chikazumi, *Physics of Ferromagnetism* (Oxford University Press, New York, 1997).
[2] J. Smith and H. P. J. Wijn, Ferrites, Philips Technical Library, (Eindhoven-Holland, 1965).
[3] V. G. Harris, Z. Chen, Y. Chen, S. Yoon, T. Sakai, A. Gieler, A. Yang, Y. He, K. S. Ziemer, N. X. Sun, C. Vittoria, J. Appl. Phys., **99**, 08M911 (2006).
[4] P. P. Hankare, R. P. Patil, K. M. Garadkar, R. Sasikala and B. K. Chougule, Mater. Res. Bull, **46**, 447 (2011).
[5] J. Kulikowski, A. Bienkowski, J. Magn. Magn. Mater. **26**, 297 (1982).
[6] Ge-Liang Sun, Jian-Bao Li, Jing Jing Sun and Xiao Zhan Yang, J. Magn. Magn. Mater. **281**, 173 (2004).
[7] N. Rezlescu, E. Rezlescu, C. Pasnicu and M. L. Craus, J. Phys.: Condens. Matter **6**, 5707 (1994).
[8] O. M. Hemeda, M. Z. Said and M. M. Barakat, J. Magn. Magn. Mater. **224**, 132 (2001).
[9] Fuxiang Cheng, Chunsheng Liao, Junfeng Kuang, Zhigang Xu, Chunhua Yan, Liangyao Chen, Haibin Zhao, and Zhu Liu, J. Appl. Phys. **85**, 2782 (1999).
[10] K. Kamala Bharathi, K. Balamurugan, P. N. Santhosh, M. Pattabiraman, and G. Markandeyulu, Phys. Rev. B **77**, 172401 (2008).
[11] K. Kamala Bharathi and G. Markandeyulu, J. Appl. Phys. **103**, 07E309 (2008).
[12] B. P. Jacob, S. Thankachan, S. Xavier and E. M. Mohammed, Phys. Scr. **84**, 045702 (6pp) (2011).
[13] Y. Q. Li, Y. Huang, S. H. Qi, F. F. Niu and L. Niu, J. Magn. Magn. Mater. **323**, 2224 (2011).
[14] H. Xiaogu, C. Jiao, W. Lixi, and Z. Qitu, Rare Metals, **30**, 44 (2011).
[15] S. E. Shirsath, S. S. Jadhav, B. G. Toksha, S. M. Patange, and K. M. Jadhav, J. Appl. Phys. **110**, 13914 (2011).
[16] Jitendra Pal Singh, Gagan Dixit, R. C. Srivastava, H. M. Agrawal and K. Asokan, J. Phys. D: Appl. Phys. **44**, 435306 (6pp) (2011).
[17] T. J. Shinde, A. B. Gadkari and P. N. Vasambekar, J Mater Sci: Mater Electron, DOI: 10.1007/s10854-011-0474-y.

[18] Muthafar F. Al–Hilli, Sean Li and Kassim S. Kassim, Mat. Chem. Phys. **128**, 127 (2011).
[19] T. J. Shinde, A. B. Gadkari and P. N. Vasambekar, J. Alloys Compd., **513**, 80 (2012).
[20] K. Kamala Bharathi, M. Noor-A-Alam, R. S. Vemuri and C. V. Ramana, RSC Adv. **2**, 941 (2012).
[21] K. Kamala Bharathi, G. Markandeyulu and C. V. Ramana, Electrochem. Solid-State Lett., **13**, G98 (2010).
[22] T. Kato, H. Mikami, and S. Noguchi, J. Appl. Phys., **110**, 123901 (2011).
[23] K. Kamala Bharathi, G. Markandeyulu and C. V. Ramana, J. Phys. Chem. C, **115**, 554 (2011).
[24] H. S. Mund, S. Tiwari, J. Sahariya, M. Itou, Y. Sakurai, and B. L. Ahuja, J. Appl. Phys., **110**, 073914 (2011).
[25] K. Kamala Bharathi, R. S. Vemuri and C. V. Ramana, Chem. Phys. Lett., **504**, 202 (2011).
[26] S. M. Chavan, M. K. Babrekar, S. S. More and K. M. Jadhav, J. Alloys Compd., **507**, 21 (2010).
[27] K. Kamala Bharathi, G. Markandeyulu and C. V. Ramana, J. Electrochem. Soc., **158**, G71 (2011).
[28] E. A. Schultz-Sikma, H. M. Joshi, Qing Ma, K. W. MacRenaris, A. L. Eckermann, V. P. Dravid, and T. J. Meade, Chem. Mater., **23**, 2657 (2011).
[29] K. Kamala Bharathi and C. V. Ramana, J. Mater. Res., **26**, 584 (2011).
[30] R. S. Devan, Y. D. Kolekar and B. K. Chougule, J. Phys.: Condens. Matter. **18**, 9809 (2006).
[31] Y. Q. Chu, Z.-W. Fu and Q.-Z. Qin, Electrochim. Acta, **49**, 4915 (2004).
[32] Y. N. Nu Li, Y. Q. Chu and Q. Z. Qin, J. Electrochem. Soc., **151**, A1077 (2004).
[33] P. Lavela and J. L. Tirado, Journal of power sources, **172**, 379 (2007).
[34] S. Ito, K. Nakaoka, M. Kawamura, K. Ui, K. Fujimoto and N. Koura, Journal of Power Sources, **146**, 319 (2005).
[35] C. H. Kim, Y. Myung, Y. J. Cho, H. S. Kim, S. H. Park, J. Park, J. Y. Kim, B. Kim, J. Phys. Chem. C, **113**, 7085 (2009).
[36] C. H. Peng, H. W. Wang, M. Z. S. Shih-Wei Kanb, Y. M. Wei and S. Y. Chen, J. Magn. Magn. Mater., **284**, 113 (2004).
[37] S. E. Ziemniak, L. M. Anovitz, R. A. Castelli and W. D. Porter, J. Phys. Chem. Solids, **68**, 10 (2007).
[38] S. S. Ata-Allah and M. Kaiser, J. Alloys Compd., **471**, 303 (2009).
[39] R. V. Mangalaraja, S. Ananthakumar, P. Manohar and F. D. Gnanam, J. Magn. Magn. Mater., **253**, 56 (2002).
[40] J. P. Zhou, H. C. He, Z. Shi and C. W. Nan, Appl. Phys. Lett., **88**, 013111 (2006).
[41] R. Hochschild and H. Fuess, J. Mater. Chem., **10**, 539 (2000).
[42] N. F. Mott and E. A. Davis, *Electronic Processes in Non-Crystalline Materials*, 2nd edn (Oxford: Clarendon, 1979).
[43] R. S. Vemuri, K. Kamala Bharathi, S. K. Gullapalli, C. V. Ramana, ACS Appl. Mater. Interfaces, **2**, 2623 (2010).